Hyperfine-structure studies of Nb II: Experimental and relativistic configuration-interaction results

L. Young, S. Hasegawa,* and C. Kurtz
Physics Division, Argonne National Laboratory, Argonne, Illinois 60439

Debasis Datta and Donald R. Beck
Physics Department, Michigan Technological University, Houghton, Michigan 49931
(Received 2 September 1994; revised manuscript received 16 January 1995)

We report an experimental and theoretical study of the hyperfine structure (hfs) in various metastable states in ^{93}Nb II. Hyperfine structures of five levels in Nb II have been measured using a combination of the laser-rf double resonance and laser-induced fluorescence methods in a collinear laser–ion-beam geometry. Theoretically, for $J=2$, a multireference calculation of energies and hfs based on a relativistic configuration-interaction methodology of the lowest ten levels in the $(4d+5s)^4$ manifold is reported. The average energy error is 450 cm^{-1}. Many of the hyperfine constants show large changes from the Dirac-Fock values and the magnetic dipole constant has a 4% accuracy for the one $J=2$ level measured. We have also identified all the core-valence and core-core effects that dominate the energy differences and hfs.

PACS number(s): 32.10.Fn, 32.30.Bv, 31.30.Gs, 31.30.Jv

I. INTRODUCTION

In this experimental and theoretical work we extend our investigation of hyperfine structure (hfs) of transition-metal $(d+s)^n$ states to the case with $n=4$, in Nb II. As in our earlier studies of two- and three-valence-electron systems, namely Sc II [1], Y II [2], Ti II [3], and Zr II [4], the experimental studies on these singly charged ions are conducted using the laser-rf double-resonance method and compared with theoretical results obtained using a relativistic configuration-interaction (CI) algorithm [5]. This study is motivated by the success of the many-body theoretical treatment for hyperfine structure at the sub-10% level in the two- [6] and three- [4,7] valence-electron cases and the desire to explore the more complex four-electron situation. An alternative *ab initio* approach to hfs is that of Hartley and Martensson-Pendrill [8], who have applied a combination of a discrete numerical basis and random-phase approximation diagrams to determine the hyperfine structure of Cs and Tl.

Theoretically, the challenge arises from the inherent complexity in these systems originating from the presence of open d electrons and $nd \leftrightarrow (n+1)s$ interchanges, which generate a pool of strongly interacting eigenstates leading to interleaved configurations. This problem has been recognized as a formidable task for some time [9–12]. Despite the complexity of these transition-metal systems and the difficulty in even obtaining the correct ordering of fine-structure levels, there has been renewed interest in the *ab initio* calculation of hfs as a test of the accuracy of the wave function near the nucleus [7,13,14]. The form of the wave function is dictated by first-order perturbation theory and its parameters (Z^*, CI coefficients) are determined by the energy variational principle [5,7,15]. Once a reasonably accurate description of the energy is obtained, the configuration-state functions important for hyperfine structure are included. The most important contributions to the energy are the pair excitations, the valence single-particle excitations, and core polarizations from the shallow core, while the only nonvanishing matrix elements of the hyperfine interaction, $H_{\rm hfs}$, are the ones arising from these single excitations as well as the inner core polarization. The hyperfine structure is calculated using first-order perturbation theory, i.e., once the coefficients associated with the single excitations are correctly established, the CI wave function is used to calculate the matrix elements of the magnetic dipole and electric quadrupole operators. In order to categorize the various classes of excitations in terms of their importance for hfs and energy differences, an extensive calculation, including all major correlations, was done iteratively for Nb II $J=2$.

Experimentally there are very few studies of the singly charged niobium ion, although such work would aid interpretation of the solar abundance of Nb from observed spectra of Nb II [16]. To our knowledge, only radiative lifetimes have previously been measured [17].

II. EXPERIMENT

The experimental apparatus shown in Fig. 1(a) for the measurement of hyperfine structure of atomic ions through the methods of laser-induced fluorescence and laser-rf double resonance has been described previously [1]. A mass-selected ^{93}Nb$^+$ beam is overlapped with a counterpropagating laser beam. Resonant interaction between the laser and ion beam is confined to well-defined regions by the postacceleration voltage. The second of these regions is used to detect laser-induced fluorescence, while the first is used only as a "pump" region to deplete the state of interest for laser-rf double-resonance mea-

*Present address: Department of Quantum Engineering and System Science, University of Tokyo, Tokyo 113, Japan.

surements, as described below. The apparatus differs from that described previously in that a modified radio frequency generation chain, as shown in Fig. 1(b), was required to measure some of the hfs intervals generated by the very large nuclear magnetic dipole moment of ^{93}Nb ($\mu = 6.167$ nm, $I = \frac{9}{2}$) [18]. For these intervals ($\nu_{rf} > 2400$ MHz), the output of the synthesizer was amplified by 28 dB, sent through a passive frequency doubler, after which a fraction (-30 dB) of the output was sent to a frequency counter, and the majority sent to a traveling-wave-tube amplifier after appropriate attenuation. The frequency-doubled, amplified output was sent directly to the rf section using a short coaxial cable. The upper frequency limit is determined primarily by the characteristics of the rf section (triplate design) [19] in the ion beamline. The 3-dB point of the rf section on the high-frequency end (≈ 2.2 GHz) was measured by analyzing the rise time of a short pulse. The useful lower frequency is limited by acceleration-deceleration effects on the ion trajectory through the rf section [20].

Nb^+ ions were produced by flowing CCl_4 vapor over Nb_2O_5 powder contained in a quartz tube that was inserted into the chamber of an oscillating-electron bombardment source. The chemical reaction occurring in the ion source chamber converts the niobium oxide to the more volatile $NbCl_5$ (mp = 204.7 °C). This eliminates the extreme temperature ($T \geq 2400$ °C required for 1 mTorr) needed to vaporize pure Nb metal (mp = 2468 °C). Nevertheless, the period required for production of a reasonable Nb^+ beam was quite long, as shown in Fig. 2. The bottom, middle, and top panels show a laser-induced fluorescence signal from Nb^+, i.e., a signal proportional to Nb^+ beam intensity, after running the source continuously for 2, 2.5, and 3 days, respectively.

Table I lists the three optical transitions studied in Nb II. These transitions were of particular interest because the lower levels, nominally of the $4d^4\,^3F$ multiplet, are highly mixed with the $4d^3 5s$ configuration and thus provide a stringent challenge to theory. Unfortunately, attempts to observe transitions from other even-parity levels, e.g., from the $4d^3 5s\,^5P$ and $4d^4\,^3G$ multiplets, resulted in spectra in which the signal-to-background ratio was insufficient for laser-rf double-resonance studies.

Figure 3 shows a typical laser-induced fluorescence spectrum for the Nb II, $4d^4\,^3F_2 - 4d^3 5p\,^3D_1^o$ transition. Optical spectra were taken by scanning the dye laser under computer control and simultaneously recording fluorescence from the ion beam and transmission through a temperature-stabilized Fabry-Pérot étalon with a free spectral range of 150.00±0.01 MHz. Typically, the opti-

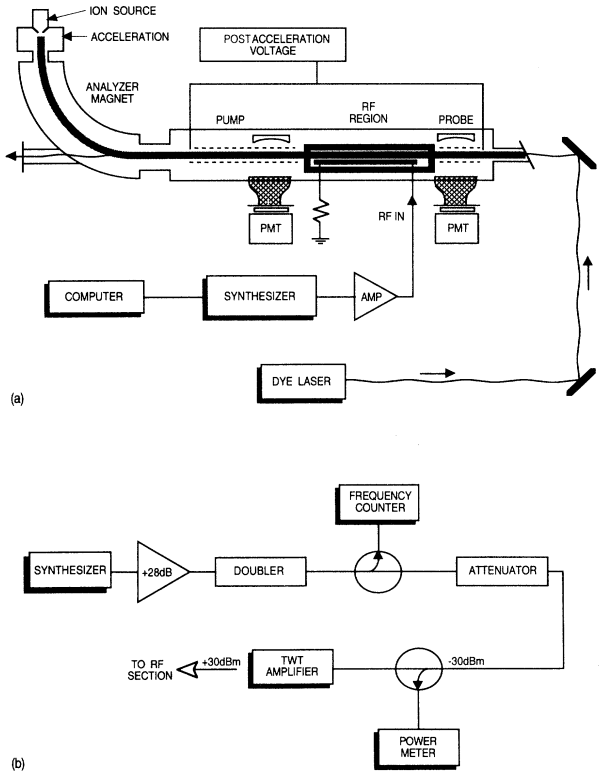

FIG. 1. (a) Standard experimental configuration for rf frequencies below 2.4 GHz. (b) Alternative radio frequency generation chain for frequencies higher than 2.4 GHz. See text for detailed description.

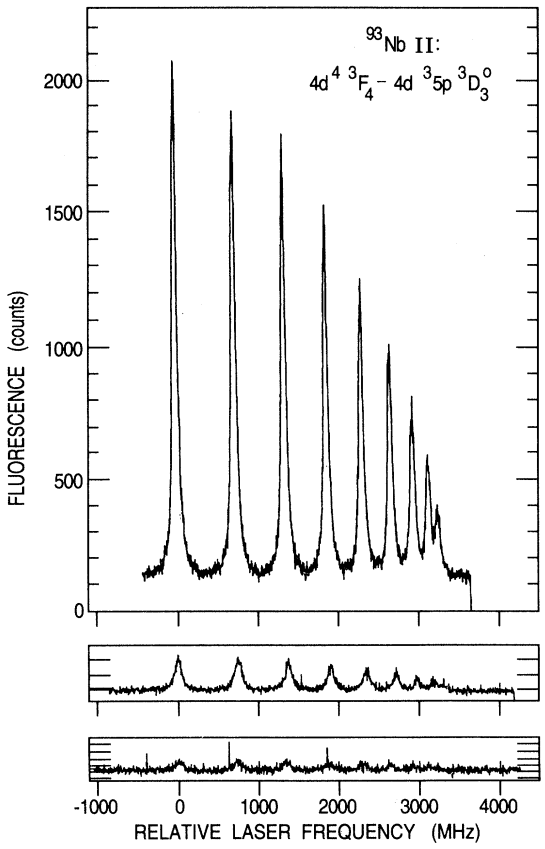

FIG. 2. Increase of Nb^+ ion-beam intensity as a function of time as monitored by laser-induced fluorescence. Lower, middle, and top panels show a laser-induced fluorescence spectrum of Nb^+ after running the source for 2, 2.5, and 3 days, respectively.

TABLE I. Optical transitions studied in $^{93}Nb^{+}$. Columns 1–3 and 4–6 give the known information about the lower and upper states, respectively [25]. Columns 7 and 8 give information about the experimental conditions used to detect the laser-induced fluorescence. *S*, *L*, and *J* designate the spin, orbital, and total angular momentum for the level.

Lower level			Upper level			Experimental parameters	
Electron configuration	*SLJ*	Excitation energy (cm^{-1})	Electron configuration	*SLJ*	Excitation energy (cm^{-1})	Laser excitation wavelength[a] (nm)	Filter used λ_{det}
$4d^4$	$^3F_2$	12 805.98	$4d^3 5p$	$^3D_1^{o\,b}$	34 886.33	452.76	3100 Å/UG 11
$4d^4$	$^3F_4$	13 665.68	$4d^3 5p$	$^3D_3^{o\,b}$	36 553.27	436.80	3000 Å/UG 11
$4d^4$	$^3F_3$	13 690.20	$4d^3 5p$	$^3D_2^{o\,b}$	35 520.83	457.94	3100 Å/UG 11

[a]The laser excitation wavelength is given for a stationary atom. In this particular experiment, the Doppler shift was typically ≈0.5 nm.
[b]The radiative lifetimes of the upper levels have been measured by Salih and Lawler, and Hannaford *et al.* [17] to be $^3D_1^o$: 5.7(3) and 5.5(3) ns; $^3D_2^o$: 5.7(3) and 5.7(3) ns; $^3D_3^o$: 5.0(3) and 5.0(3) ns.
[c]Schott® filter glass designation.

cal spectra had linewidths of ≈60 MHz and were taken at low laser intensity to avoid power broadening. Spectra from each of the transitions listed in Table I were analyzed and used as starting points in the search for rf resonances.

Radio frequency transitions were detected in the pump-rf-probe configuration. The hyperfine level of interest is depleted through optical pumping in the "pump" region. Subsequently, the radio frequency applied to the resonance region is scanned to produce an increase in fluorescence in the probe region when repopulation from a neighboring hyperfine level occurs. A typical rf transition is shown in Fig. 4. It exhibits the Rabi two-level line shape and has a full width at half maximum of approximately 500 kHz, determined by the transit time through the rf interaction region. As can be seen from the geometry of the laser and rf interaction regions, the optical field is present in the rf region, giving rise to the possibility of ac Stark shifts [21]. For this reason, the postacceleration voltage applied to the optical interaction regions were carefully selected to ensure that the optical field was at least 2 GHz from resonance (Doppler shift $=\nu_0/\sqrt{2mE}\approx 7.4$ MHz/V, where ν_0 is the frequency of the optical field, m is the ion mass, and E is the energy of the ion). The significance of the Stark shifts was estimated by measurements of the $^3F_4$ hfs intervals with the observation region biased at −80 V as opposed to −300 V relative to ground. In these measurements the rf resonances were shifted systematically to lower frequencies by 6 to 23 kHz at the −80-V bias with a laser intensity of approximately 300 mW/cm^2. A linear extrapolation of the shifts observed at −80 V to the nominal −300-V bias used for measurement would render them within the statistical accuracy of a rf resonance, typically ≈6 kHz. The statistical error was determined by the standard deviation of eight measurements of each interval, four with

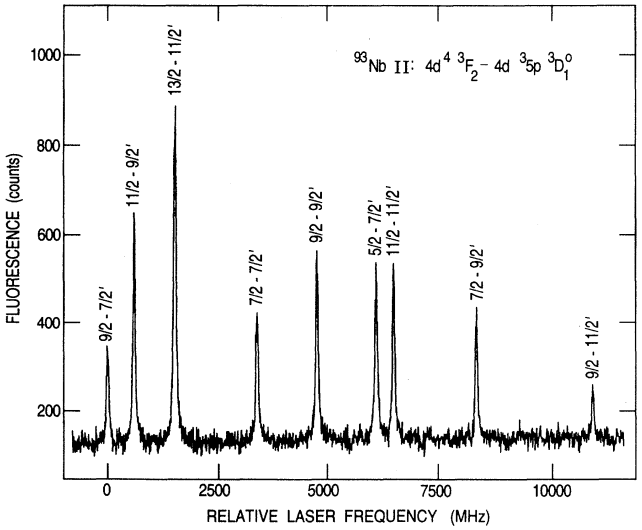

FIG. 3. A typical laser-induced fluorescence spectrum for the $4d^4\,^3F_2$–$4d^3 5p\,^3D_1^o$ transition in Nb II. The linewidths are typically 60 MHz. Primes denote upper state *F* value.

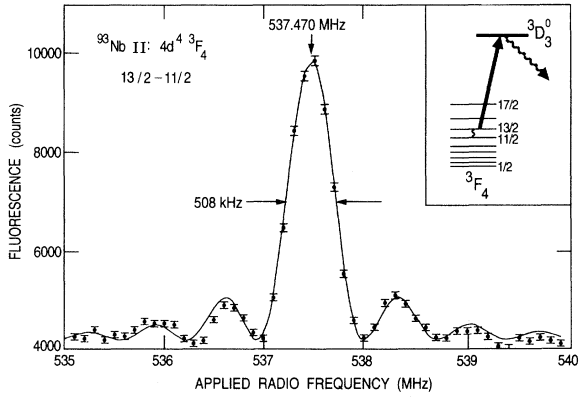

FIG. 4. A radio frequency resonance for the $F=\frac{13}{2}-\frac{11}{2}$ interval in the $4d^4\,^3F_4$ state of Nb II. The inset shows the hyperfine structure for the $4d^4\,^3F_4$ lower state. The straight arrow represents the laser transition to the upper $^3D_3^o$ state (for which the hfs is not optically resolved, as seen in Fig. 2). The wavy arrow denotes fluorescence to other levels which is detected. The wiggly line represents the applied rf radiation between the $F=\frac{13}{2}$ and $F=\frac{11}{2}$ levels.

TABLE II. Observed and calculated hfs intervals for levels studied by laser-rf double resonance in the $4d^4$ configurations of $^{93}Nb^+$. The fourth column designates the upper and lower hyperfine levels for the measured interval. In the fifth column, the numbers in parentheses represent one standard deviation of the mean. The values in the sixth column are calculated from the A and B values listed in Table III.

Excitation energy (cm^{-1})	Electron configuration	SLJ	$F-F'$	ν_{obs} (MHz)	ν_{calc} (MHz)	$\nu_{obs}-\nu_{calc}$ (MHz)
12 805.98	$4d^4$	$^3F_2$	5/2–7/2	2654.736(8)	2654.736	0.000
			7/2–9/2	3412.235(15)	3412.235	0.000
13 665.68	$4d^4$	$^3F_4$	9/2–11/2	444.332(4)	444.403	−0.072
			11/2–13/2	536.895(3)	536.862	0.034
			13/2–15/2	635.232(4)	635.149	0.083
			15/2–17/2	740.109(2)	740.162	−0.053
13 690.20	$4d^4$	$^3F_3$	7/2–9/2	1881.283(8)	1881.236	0.046
			9/2–11/2	2305.971(6)	2305.997	−0.026
			11/2–13/2	2734.740(4)	2734.783	−0.043
			13/2–15/2	3168.353(4)	3168.325	0.028

the beam and rf propagation parallel and four antiparallel. The geometric average of the parallel and antiparallel resonance is reported in Table II, with the standard deviation of each measurement in parentheses.

In Fig. 5 the three lower levels studied, $^3F_{4,3,2}$, are diagrammed in boldface along with other levels in the 12 000–14 000 cm^{-1} range. As can be seen from the energy-level diagram, this multiplet is not in the standard order (increasing $J \rightarrow$ increasing E), nor is it grouped together, with members of the ^3D multiplet interspersed. It also shows that the $^3F_2$ level is reasonably well isolated in comparison to the $^3F_4$ and $^3F_3$. On the right-hand side of Fig. 5 the measured hyperfine intervals are shown on an enlarged scale ($\approx \times 1300$). The wiggly lines represent intervals that have been measured in this work.

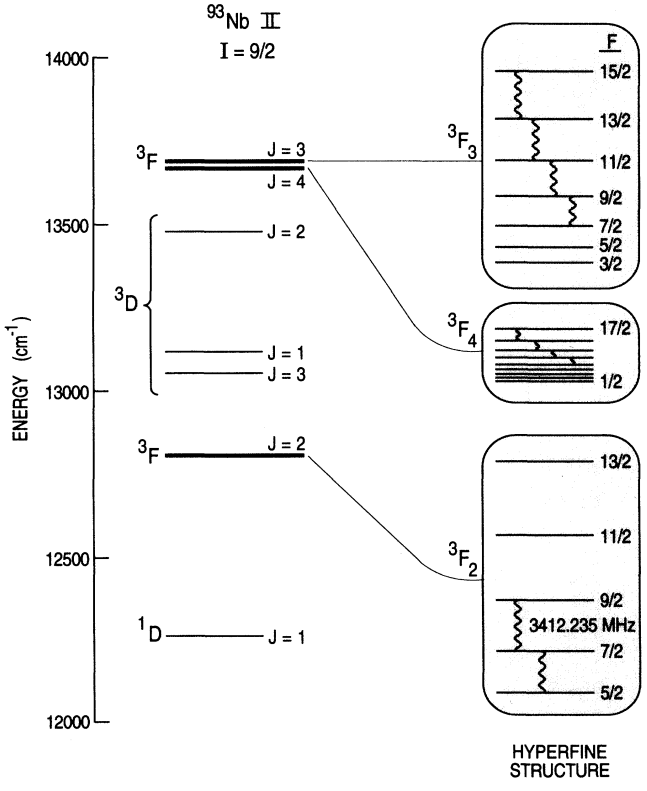

FIG. 5. An energy-level diagram in the region of experimental data. The three levels for which rf transition were measured are shown in bold. The enlarged scale on the right ($\approx \times 1300$) shows the hyperfine structure associated with each of these levels. The wiggly lines represent the actual rf transitions measured.

III. EXPERIMENTAL RESULTS AND ANALYSIS

The magnetic dipole A and electric quadrupole B interaction constants are determined from the standard hfs formula given by Schwartz [22]. For the lower levels, the hfs intervals determined by rf resonance, listed in Table II, are used in conjunction with the ordering determined by the laser-induced fluorescence spectra to determine the A's and B's. The results obtained by linear least-squares fitting are shown in Table III. The A and B values are used to calculate the intervals listed in the sixth column of Table II. It is clear from the residuals

TABLE III. Magnetic dipole (A) and electric quadrupole (B) hfs constants in MHz determined for $^{93}Nb^+$ levels by laser-rf double resonance for even-parity levels and by laser-induced fluorescence for odd-parity levels. The numbers in parentheses represent estimated uncertainties of one standard deviation.

Excitation energy (cm^{-1})	Electron configuration	SLJ	A (MHz)	B (MHz)
12 805.98	$4d^4$	$^3F_2$	757.998(8)	−3.99(7)
13 665.68	$4d^4$	$^3F_4$	82.893(6)[a]	100.436(184)[a]
13 690.20	$4d^4$	$^3F_3$	420.004(3)[a]	43.908(81)[a]
34 886.33	$4d^35p$	$^3D_1^o$	1059.73(69)	6.4(3)
35 520.83	$4d^35p$	$^3D_2^o$	203.81(38)	16.1(6)

[a]The standard deviation was calculated using the difference between the observed and calculated frequencies as the error in the measurement. These differences are between 4 and 27 times larger than the statistical error in the measurement and thus yield correspondingly larger errors in the derived A's and B's.

shown in the rightmost column of Table II that for the $^3F_4$ and $^3F_3$ levels there are significant deviations ($>2\sigma$) from the two-parameter fit to the hfs intervals. These deviations are most likely due to second-order corrections from hyperfine mixing of states of the same F but different J. Since the deviations are on the tens of kilohertz scale, these second-order corrections make only minor perturbations on the A's and B's (0.007% and 0.18% for the A and B, respectively). The uncertainty for the $^3F_3$ and $^3F_4$ levels quoted in Table III therefore corresponds to that evaluated using the residuals ($-0.072, 0.034...$ MHz) as the uncertainty in the measured value. For the $^3F_2$ level second-order perturbations are expected to be substantially smaller, since the level is quite isolated (see Fig. 5), and therefore the statistical uncertainty is used.

IV. RELATIVISTIC CI CALCULATIONS

The focus of our theoretical calculation was the $J=2$ family, since it gives rise to the maximum number of levels in the $(d+s)^4$ manifold. The Hamiltonian is the Dirac-Coulomb Hamiltonian with Breit magnetic and retardation corrections. The wave function is built as a linear combination of orthonormal configuration-state functions each of which is an eigenstate of J^2 and J_Z. The radial parts of the occupied spinors are obtained as numerical solutions to the multiconfiguration Dirac-Fock (MCDF) equations [23], while those for the unoccupied spinors are the analytic screened relativistic hydrogenic functions and are parametrized through their effective charge Z^*.

The many-body configurations are generated by single and double excitations from all the $4d^4$, $4d^35s$, and $4d^25s^2$ reference states, and include the dominant core-valence and core-core pairs. This is specially important because the near degeneracy of the $4d$ and $5s$ orbitals causes many of the atomic states to be an admixture of these valence configurations and may strongly affect their hyperfine structure. All possible single and double excitations from the $4s$, $4p$, $4d$, and $5s$ orbitals have been examined, and only those configurations that determine the relative position of the energy levels and influence the hyperfine structure have been retained. We give here a brief account of the most important correlation phenomena for the low-lying (bottom ten roots) levels; a detailed account will be given elsewhere [24]. The dominant corrections to the energy come from the $(4d+5s)^2 \rightarrow dd, ff, pf$; $4p^2 \rightarrow 4d^2+4dd$, the $4p4d \rightarrow pd, df, fg$ pairs, and also from the $4p \rightarrow p, f$ singles. In addition to the above, the $4s, 5s \rightarrow s$ excitations are crucial for the hfs, although they are not important for energy considerations. As was also noted in our prior work on Zr II [7], the so-called exclusion effects, viz. $4p^2 \rightarrow 4d^2+4dd$ are found to be of singular importance in determining the relative position of the energy levels, along with other core-valence effects ($4p4d \rightarrow$) and shallow-core polarizations ($4p \rightarrow p, f$). The final wave function consists of excitations $4d, 5s \rightarrow s, d, g$; $(4d+5s)^2 \rightarrow ss, pp, dd, ff, gg, sd, pf, dg$; $4p^2 \rightarrow 4d^2+4dd, 4p(4d+5s) \rightarrow pd, df, fg$; $4p, 3p \rightarrow p, f$, and $4s, 3s \rightarrow s, d$ generated from

TABLE IV. CI energies and hyperfine structure of Nb II $J=2(d+s)^4$ states. Only the lowest ten roots are listed. A dagger (†) indicates that the theory differs from the level designations given in Moore [25]. For the values in the fourth column, 438.38 cm^{-1} has been added to give level positions relative to the actual ground state. In the fifth and sixth columns, the MCDF values are given within parentheses for comparison to the RCI values. L and S designate the orbital and spin angular momenta of the state.

Level (Ref. [25])		Energy (cm^{-1})		Theoretical hfs constants		Theoretical level composition (Ref. [24])	
Configuration	$^{(2S+1)}L$	Experiment	Theory	A (MHz)	B (MHz)/$Q(b)$	Dominant configuration	Leading LS (%)
$4d^35s$	^3D	19 351.98	20 008.58	490.55 (625.03)	−130.50 (−107.69)	$4d^35s$	88.3 ^3D
$4d^35s$	^3P	14 660.77	14 815.08	610.41 (863.39)	71.42 (40.60)	$4d^35s$	82.4 ^3P
$4d^4$ †	^3D	13 479.50	14 095.28	878.34 (740.67)	−208.04 (−149.86)	$4d^35s$	64.7 ^3F
$4d^4$ †	^3F	12 805.98	13 441.68	729.32 (785.59)	56.99 (27.63)	$4d^4$	64.0 ^3D
$4d^4$	^1D	12 263.26	12 896.38	163.39 (82.99)	20.98 (90.57)	$4d^4$	79.3 ^1D
$4d^35s$	^5P	10 835.85	10 481.98	1808.69 (1509.67)	−294.46 (−255.13)	$4d^35s$	89.0 ^5P
$4d^35s$ †	^3F	7505.78	8118.78	892.13 (541.05)	−71.55 (−44.43)	$4d^4$	91.5 ^3F
$4d^4$	^3P	7261.33	7438.68	194.35 (300.13)	24.83 (17.22)	$4d^4$	90.8 ^3P
$4d^35s$	^5F	2629.07	2378.28	454.81 (407.37)	−42.24 (−37.99)	$4d^35s$	92.5 ^5F
$4d^4$	^5D	438.38	438.38	−160.58 (104.73)	88.92 (81.18)	$4d^4$	94.4 ^5D

all the eigenvectors in the $(4d+5s)^4$ manifold. Their combined effects yield an energy spectrum that resembles the experimental spectrum very closely. Due to limitations in the available memory size and disk space, a somewhat restricted eigenvector set was used; by enhancing the set, further refinements may be possible. On a Sparcstation10 the final CI run took close to 33 h having a matrix of dimension 6559 and using a preoptimized radial basis.

The average error in the energies for the bottom ten levels is ≈ 450 cm^{-1} (Table IV), much improved over the accuracy achieved (≈ 705 cm^{-1}) for the Zr II $J=\frac{3}{2}$ levels [4]. Most of these states are quite pure ($>79\%$) and agree with the labeling used in Moore's tables [25]. However, we find the seventh and eighth roots (the $4d^4\,{}^5D$ reference being the first) to be $4d^4({}^3D+{}^3F)$ and $4d^3 5s({}^3F+{}^3D)$, respectively. Also, the $4d^3 5s\,{}^3F$ level is actually dominated by the $4d^4$ configurations. Theoretical assignments of the levels are given in the extreme right-hand columns of Table IV.

The magnetic dipole A and electronic quadrupole B hyperfine constants have been calculated for all ten levels. Some of the dipole constants show large changes from their MCDF values, including a sign flip for the $4d^4\,{}^5D$ reference state. For the only level $[4d^4({}^3D+{}^3F)]$ for which a measurement has been made, the agreement in A is excellent ($<4\%$). Accuracy estimates for the remaining levels and hyperfine predictions for the higher levels will be given in Ref. [24].

Many of the electronic quadrupole hyperfine constants also show significant changes from the MCDF values. Comparing the theoretical B/Q and experimental B for the only level measured, the computed nuclear quadrupole moment Q does not agree very well with the known value [18] of Q. A study of positive and negative correlation contributions to B shows cancellation effects to be highest for this level, effectively yielding a difference only $<1\%$ of the total absolute contribution, thus making an accurate theoretical calculation extremely difficult. The accuracy of the rest of the values can be judged only after experimental results for them are available.

V. CONCLUSION

An experimental and theoretical study of hyperfine structure in the metastable levels of Nb II has been completed. The laser-rf double resonance and laser-induced fluorescence methods were used to measure A and B hfs constants for five levels. The A and B of one measured level, $4d^4\,{}^3F_2$, were compared to the results of our fully *ab initio* multireference relativistic configuration-interaction (RCI) calculation for the $J=2$ levels. In this calculation, the energies and hyperfine-structure constants of the lowest ten levels of the Nb II $J=2$ $(4d+5s)^4$ manifold were evaluated. They show excellent agreement with experimental energy values (≈ 450 cm^{-1} average discrepancy). For three levels we also correct the configurational assignments given in Moore [25]. The RCI hfs constants in general show large changes from the Dirac-Fock values. For the one comparison possible between experiment and theory, the magnetic dipole interaction constant is accurate to 4%, while the electric quadrupole interaction constant is in poor agreement with experiment due to large cancellations in many-body effects. The predicted accuracy of the other calculated A values is $\geq 5\%$, and the verification of such awaits further experimental data.

ACKNOWLEDGMENTS

We thank W. J. Childs for valuable comments and interest in this work. D.R.B. and D.D. thank the Division of Chemical Sciences, Office of Energy Research, U.S. Department of Energy, Grant No. DE-FG02-92ER14282 for support of this work. S.H. thanks the U.S.-Japan Student Exchange Program of the American Nuclear Society and the Atomic Energy Society of Japan for support. This research was supported by the U.S. Department of Energy, Office of Basic Energy Science, under Contract No. W-31-109-ENG-38.

[1] L. Young, W. J. Childs, T. Dinneen, C. Kurtz, H. G. Berry, L. Engstrom, and K. T. Cheng, Phys. Rev. A **37**, 4213 (1988); N. B. Mansour, T. Dinneen, L. Young, and K. T. Cheng, *ibid.* **39**, 5762 (1989).
[2] T. P. Dinneen, N. Berrah Mansour, C. Kurtz, and L. Young, Phys. Rev. A **43**, 4824 (1991).
[3] N. B. Mansour, C. Kurtz, L. Young, D. R. Beck, and D. Datta, Phys. Rev. A **46**, 5774 (1992).
[4] L. Young, C. Kurtz, D. R. Beck, and D. Datta, Phys. Rev. A **48**, 173 (1993).
[5] D. R. Beck, Phys. Rev. A **37**, 1847 (1988).
[6] D. R. Beck, Phys. Rev. A **45**, 1399 (1992).
[7] D. R. Beck, and D. Datta, Phys. Rev. A **48**, 182 (1993).
[8] A. C. Hartley and A. M. Martensson-Pendrill, Z. Phys. D **15**, 309 (1990).
[9] C. Froese-Fischer, J. Phys. B **10**, 1241 (1977).
[10] C. W. Bauschlischer, J. Chem. Phys. **86**, 5591 (1987).
[11] T. H. Dunning, B. H. Botch, and J. F. Harrison, J. Chem. Phys. **72**, 3419 (1980).
[12] R. B. Murphy and R. P. Messmer, J. Chem. Phys. **97**, 4974 (1992).
[13] P. Villemoes *et al.*, Phys. Rev. A **45**, 6241 (1992); P. Jönsson, Phys. Scr. **48**, 678 (1993).
[14] J. Bieron, F. A. Parpia, C. Froese-Fischer, and P. Jönsson (unpublished).
[15] Z. Cai, D. R. Beck, and W. F. Perger, Phys. Rev. A **43**, 4660 (1991).
[16] O. Hauge and N. H. Youssef, Solar Phys. **41**, 67 (1975).
[17] S. Salih and J. E. Lawler, Phys. Rev. A **28**, 3653 (1983); P. Hannaford, R. M. Lowe, E. Biémont, and N. Grevesse, Astron. Astrophys. **143**, 447 (1985).
[18] G. H. Fuller, J. Phys. Chem. Ref. Data **5**, 835 (1976).
[19] A. Sen, L. S. Goodman, and W. J. Childs, Rev. Sci. Instrum. **59**, 74 (1988).

[20] L. Young, T. Dinneen, and N. B. Mansour, Phys. Rev. A **38**, 3812 (1988).
[21] G. Borghs, P. DeBisschop, J. Odeurs, R. E. Silverans, and M. Van Hove, Phys. Rev. A **31**, 1434 (1985).
[22] C. Schwartz, Phys. Rev. **97**, 380 (1955).
[23] J. P. Desclaux, Comput. Phys. Commun. **9**, 21 (1975).
[24] D. Datta and D. R. Beck (unpublished).
[25] C. E. Moore, *Atomic Energy Levels,* Natl. Bur. Stand. (U.S.) Circ. No. NSRDS-NBS35 (U.S. GPO, Washington, DC, 1971), Vol. II.

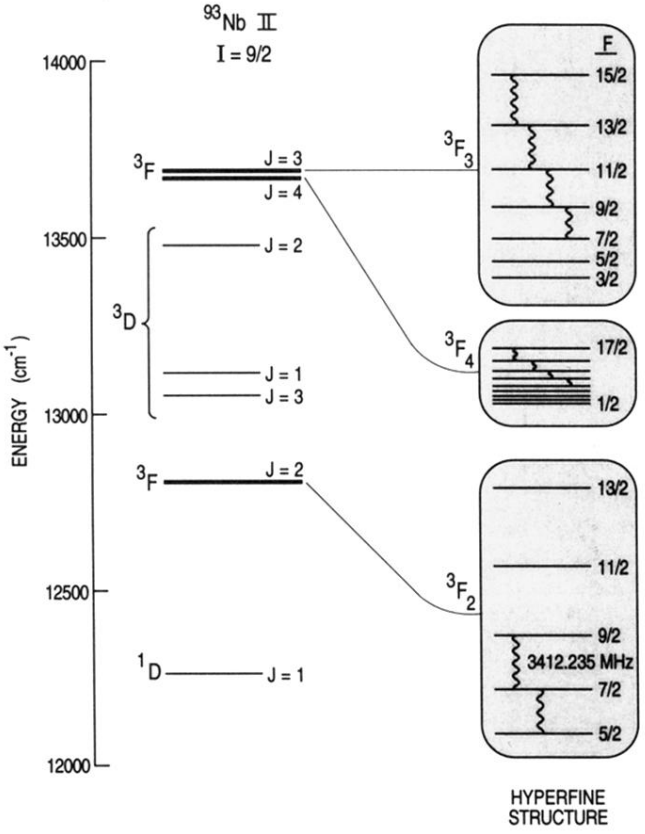

FIG. 5. An energy-level diagram in the region of experimental data. The three levels for which rf transition were measured are shown in bold. The enlarged scale on the right ($\approx \times 1300$) shows the hyperfine structure associated with each of these levels. The wiggly lines represent the actual rf transitions measured.